

See discussions, stats, and author profiles for this publication at: <https://www.researchgate.net/publication/244467455>

Nonradiative Excitation Fluorescence: Probing Volumes Down to the Attoliter Range

ARTICLE *in* JOURNAL OF PHYSICAL CHEMISTRY LETTERS · AUGUST 2010

Impact Factor: 7.46 · DOI: 10.1021/jz100917u

CITATIONS

9

READS

41

4 AUTHORS, INCLUDING:



Pascale Winckler

University of Burgundy

16 PUBLICATIONS 44 CITATIONS

[SEE PROFILE](#)



Jérôme Plain

Université de Technologie de Troyes

123 PUBLICATIONS 1,168 CITATIONS

[SEE PROFILE](#)

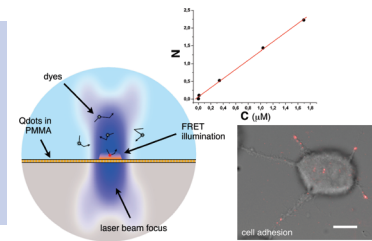
Nonradiative Excitation Fluorescence: Probing Volumes Down to the Attoliter Range

Pascale Winckler, Rodolphe Jaffiol,* Jérôme Plain,* and Pascal Royer

Laboratoire de Nanotechnologie et d'Instrumentation Optique, LRC CEA, CNRS UMR 6279 - STMR, Institut Charles Delaunay, Université de Technologie de Troyes, 12 rue Marie Curie, BP 2060, 10 010 Troyes cedex, France

ABSTRACT We develop a new active substrate, allowing us to excite nonradiatively labeled fluorescent biosamples. We demonstrate the potential of our method through two biological relevant applications, that is, direct imaging of the cell adhesion points and single-molecule spectroscopy at high (micromolar) concentration.

SECTION Kinetics, Spectroscopy



Both single-molecule imaging and single-molecule spectroscopy are becoming standard analytical methods in chemistry and biology. The rise in popularity of single-molecule techniques in biology is mainly due to the association of time-resolved fluorescence spectroscopy, such as fluorescence correlation spectroscopy (FCS), with confocal microscopy.^{1,2} In this usual approach, the dimension of the laser beam focal point, together with the use of a confocal pinhole, defines the observation volume from which the fluorescence is collected. However, the diffraction barrier with such a far-field microscopy technique appears to be a critical issue for FCS applications in life sciences. Consequently, some recent advances in nanoscale imaging arouse a strong interest within the biology community, since they offer a true and efficient alternative to well-established techniques (photonic structures, excitation beam design, and so forth).^{3–9} Here, we present a new method of local illumination involving a non-radiative energy transfer, which improves the out-of-plane spatial resolution by several orders of magnitude, reducing the effective excitation volume to the attoliter level. Nonradiative energy transfer refers to Förster resonance energy transfer (FRET) from excited donors (quantum dots in our case) to acceptors (organic dyes).¹⁰ This well-known physical process strongly depends on the interdistance between donors and acceptors (typically a few nanometers), allowing a drastic reduction of the excitation volume. In this Letter, we present two biologically related applications based on this new illumination scheme. The first one concerns single-molecule FCS experiments at biologically relevant concentrations, typically from 0.1 to 1 μM or higher. The second one relies on the high-resolution observation in wide-field imaging of the adhesion points of living cells.

To break the diffraction limit, we propose an easy method exclusively based on the activation of the substrate allowing a local excitation of the fluorescent molecules present in the biological sample through a FRET mechanism. The cover glass surface is activated with a thin film of PMMA (thickness \approx 10 nm), highly doped with quantum dots (QDs) (see Supporting Information). This activated substrate simply replaces the standard coverslip, while the rest of the fluorescent

microscope remains unchanged. To reach the nanoscale resolution, the dyes will not be excited directly by the laser source, as in a classical illumination scheme, but through a nonradiative energy transfer. The FRET process is characterized by the Förster distance R_0 , which corresponds to an attenuation of 50 % of the transfer efficiency. As shown by T. Förster,¹¹ R_0 can be calculated from the spectral overlap between donor emission and acceptor absorption, Figure 1A. We found $R_0 \approx 9.5$ nm for QDs—FortOrange in PMMA as donors and Alexa647 in water as acceptors (see Supporting Information). Therefore, through the FRET process, the QD-based functionalization of the substrate actually offers to any conventional microscope an increase of the out-of-plane spatial resolution and a strong spectral selectivity. Furthermore, the use of QDs as donors presents two advantages for biological investigations. First, a QD gives the opportunity to make long time observations since it presents a high photostability in regards to photobleaching. The second advantage is the important Stokes shift between the blue excitation of the QDs and the acceptor emission, as shown in Figure 1A. This important Stokes shift avoids direct excitation of the acceptor with the laser source. Moreover, by limiting the detection spectral window to the emission of the acceptor (Figure 1A), the autofluorescence of cells, which is the most important source of background in vivo studies, is definitively eliminated (see Supporting Information).

The first application that we present concerns fluorescence correlation spectroscopy (FCS), which is a well-established technique in biology to investigate diffusion, fluidity, local concentration, interaction between molecules, and binding reactions in living cells.^{1,2,12} Currently, the majority of FCS experiments were carried out using a confocal microscope, which works at a very low concentration of dyes (typically lower than 50 nM). This last condition reduces considerably the field of application of FCS, in particular, for medicine and

Received Date: July 6, 2010

Accepted Date: July 26, 2010

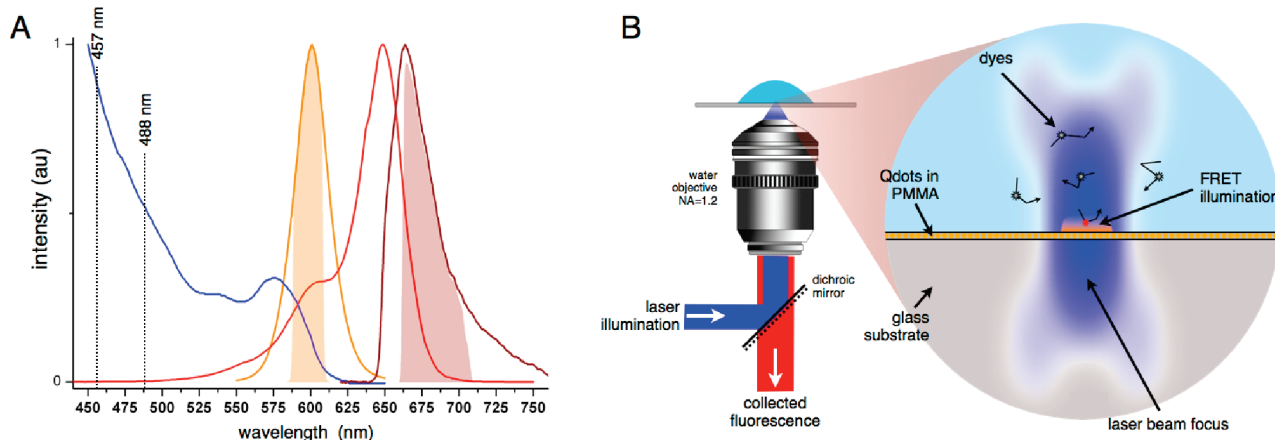


Figure 1. (A) Normalized absorption and emission spectra of the donor (QD: blue and orange) and acceptor (Alexa647: red and brown). The colored areas in orange and in brown represent the spectral detection windows of the two detection channels of our optical setup. One channel is dedicated to the donor (in orange) and the other one to the acceptor (in brown) (see Supporting Information). The two vertical dotted lines give the spectral location of the two laser lines used. (B) Scheme of our experimental approach, showing the drastic reduction of the illumination depth achieved through the nonradiative energy transfer.

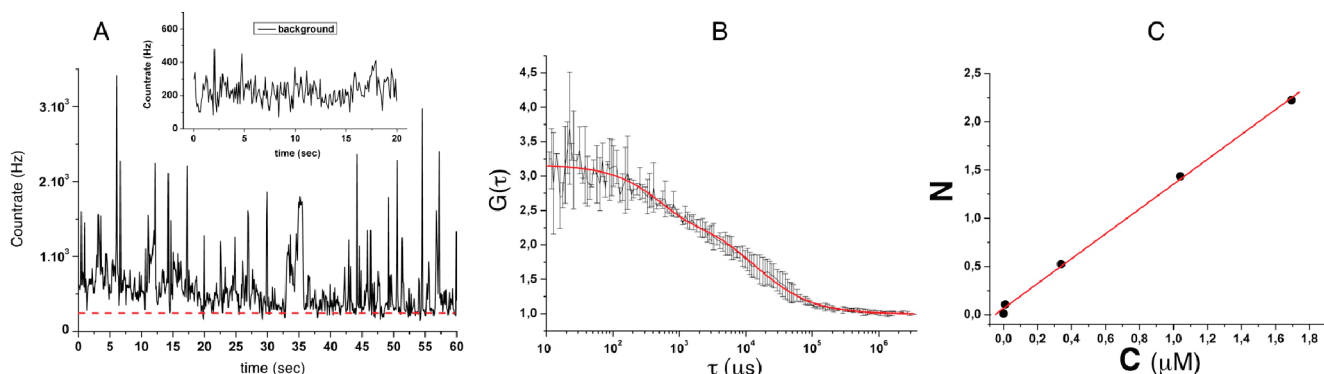


Figure 2. (A) Typical fluorescence time trace recorded on a solution of Alexa647 in water ($C = 340\text{nM}$) excited via nonradiative energy transfer. The laser power at 488 nm, measured at the pupil entrance of the water objective, is 100 nW. The red dashed line gives the mean level of the background signal (~220 Hz in this example). The inset is the background signal recorded on the same solution of Alexa647, under the same experimental conditions (100 nW at 488 nm), but without QDs onto the surface. (B) Autocorrelation curve $G(\tau)$ obtained with the same solution of Alexa647. This curve results from the average of several autocorrelation curves recorded in different places on an activated substrate. The dots represent the mean and the error bars the standard deviation. The red curve is the fit according to a 2D diffusion model (see Supporting Information). In this example, the fluorescence signal per molecule is typically $\sim 1\text{ kHz}$. (C) Plot of the mean number N of detected molecules against the concentration C of Alexa647 solutions. The red curve is the linear fit according to the general equation, independent of the shape of the observation volume, $N = C \cdot V$.

pharmacology studies, where the typical concentrations of drugs are in the micromole (μM) range or higher. One of the driving forces of the FCS community is to develop new strategies and techniques to bypass this limitation by reducing the observation volume size, as recently reviewed.¹³

In our FCS experimental configuration (Figure 1B), an argon laser beam is focused through a high numerical aperture water objective. The activated surface is locally excited, as illustrated in Figure 1B. The energy transfer only occurs when the freely diffusing acceptor molecules are situated in the vicinity of the surface. FRET gives rise to fluorescence emission from dye acceptors, which is collected through the same objective and sent on to an avalanche photodiode. In this excitation scheme, the depth of the effective illumination is given by R_0 and is typically lower than 15 nm, as illustrated in Figure 1B.

Figure 2A represents a typical fluorescence time trace recorded in a concentrated solution of Alexa647 (340nM) using a nonradiative illumination scheme. It clearly appears from our measurements that FRET illumination gives rise to fluorescence bursts from acceptors. The signal-to-noise ratio is very good; the background is about 10 % of the total detected signal (see Supporting Information). Figure 2B shows the corresponding autocorrelation function $G(\tau)$, which is fitted using a 2D diffusion model (see Supporting Information). The autocorrelation functions are exploitable on a very broad range of concentrations, typically from $\sim 1\text{ nM}$ to $\sim 2\text{ }\mu\text{M}$ (over 3 orders of magnitude), which is the highest practical range ever reported.¹³ Since the amplitude of $G(\tau)$ is inversely proportional to the mean number N of dyes simultaneously present in the observation volume, we obtain from the plot of the mean number of molecule versus the concentration the

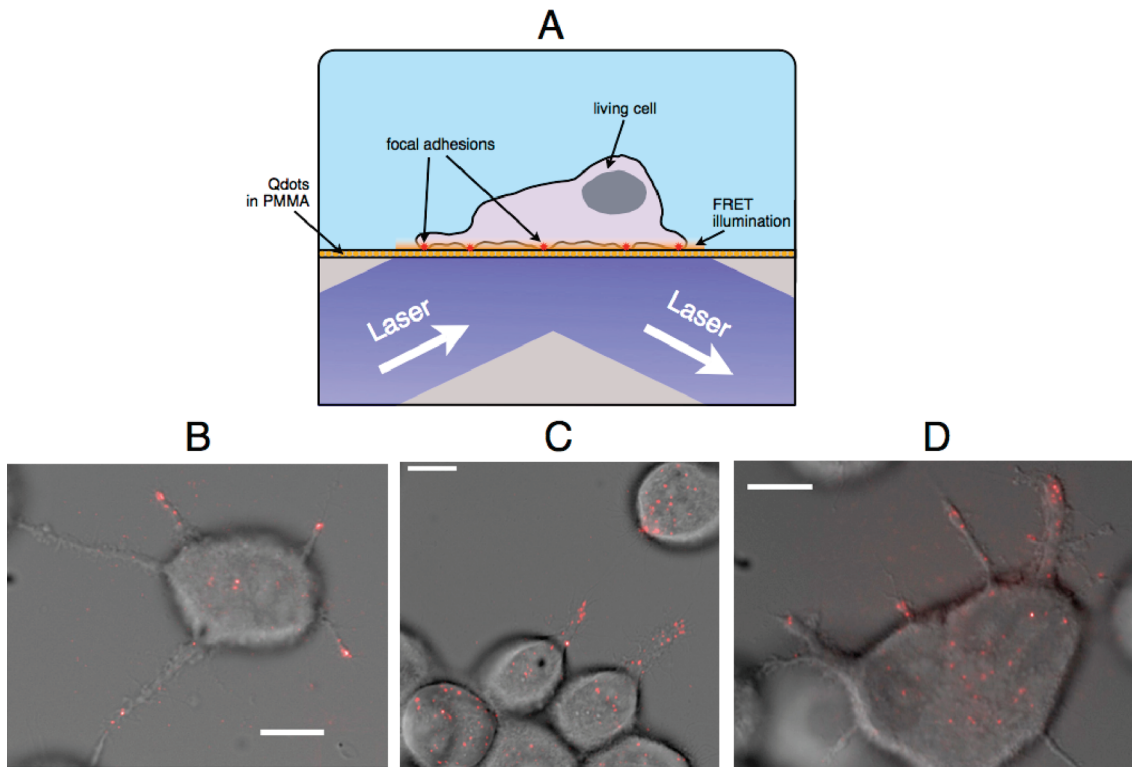


Figure 3. (A) Illustration of the wide-field FRET illumination scheme under a living cell (see Supporting Information). The red stars represent the cell–surface links. (B), (C), and (D) are three typical adhesion pictures obtained with MCF7 cells at room temperature ($\sim 22^\circ\text{C}$). These images are the superposition of two different images recorded consecutively. First in red scale, a fluorescent image obtained by FRET illumination with a laser excitation at 457 nm (typical exposure time: 100–200 ms; laser intensity: $10\text{--}20 \text{ W/cm}^2$). Second in gray scale, a differential interference contrast (DIC) image of the same area. The white bar represents the scale, $10 \mu\text{m}$.

actual size V of the observation volume. Working at well-controlled concentrations, it is easy to deduce V from the slope of the plot of $N(C)$ in Figure 2C. We find an observation volume of about 2.15 ± 0.05 attoliter, which corresponds to a volume about 200 times smaller than the conventional confocal volume measured with an excitation wavelength at 632.8 nm (see Supporting Information).

This new illumination scheme can also be exploited in fluorescence imaging. As a second application, we present a study of cell adhesion, which is a key issue in understanding the assembly of individual cells into 3D tissues. As far as we know, two major optical techniques are currently used to tackle this problem. The first one is reflection interference contrast microscopy (RICM) and its related methods, which allows one to measure plasma membrane to surface distances with a nanometric precision.¹⁴ The second strategy combines total internal reflection fluorescence microscopy (TIRFM) with a specific labeling of proteins involved in adhesion process (integrin, FAK, and so forth).¹⁵ Our nonradiative illumination scheme presents many advantages in regards to biological observations. First, activated surfaces are completely biocompatible. Second, they are designed to fit with conventional bright-field imaging in biology, such as phase contrast or differential interference contrast (DIC) imaging. Third, no specific adhesion protein labeling is required.

The well-known plasma membrane probe DilC₁₈(5) oil (DiD) is chosen as the acceptor in this experiment. As

previously explained, only areas of the plasma membrane of cells in close contact with the surface are excited by FRET and then fluoresce. Figure 3A presents schematically our approach for the cell adhesion observations, where MCF-7 human breast cancer cells are used. Interactions between cells and the surface involve strong contact (named focal adhesion) through the multiprotein functional unit linked to actin filaments and soft contact (without specific mediated-protein interactions). Figure 3B–D shows typical pictures obtained with different cells under incident illumination at 457 nm. The fluorescence images are superimposed with classic DIC pictures recorded on the same area. Thus, it clearly appears by colocalization that adhesion points are preferentially situated at the extremity of the filopodia and lamellipodia and under the body of the cell. Moreover, coupled to a highly sensitive CCD camera, our system enables us to follow dynamically the contact displacements in time (see the movie in Supporting Information).

Our results demonstrate that illumination based on nonradiative energy transfer is a simple implementation and powerful technique for reducing the confocal volume by about 2 orders of magnitude. This reduction, due to the drastic reduction along the optical axis (from $2 \mu\text{m}$ to 10 nm), allows us to increase the label's concentration range drastically for FCS experiments, thus covering 3 orders of magnitude, which is the widest range ever reported. In parallel, we have shown the relevance of our method for the study of adhesion of cells,

allowing a direct visualization of the adhesion areas. This paves the way for a better understanding of the cell adhesion, migration, and coalescence. Furthermore, the blinking of QDs, which currently limits studies on a single quantum dot, can be broken by using new nonblinking nanocrystals, like those recently reported in the literature,¹⁶ and thus opens the way to reduce the confocal volume in the three directions.

SUPPORTING INFORMATION AVAILABLE The description of the material and methods, the advantages of quantum dots for FRET applications, and an analysis of the signal-to-noise ratio in FRET illumination. This material is available free of charge via the Internet at <http://pubs.acs.org>.

AUTHOR INFORMATION

Corresponding Author:

*To whom correspondence should be addressed. E-mail: rodolphe.jaffiol@utt.fr (R.J.), jerome.plain@utt.fr (J.P.).

ACKNOWLEDGMENT This work was supported by the French National Research Agency (Contract No. ANR-JC07_190015/ANR-07-JCJC-0154). We thank P. Jeannesson and H. Morjani from the University of Reims, France, for providing the living cells.

REFERENCES

- (1) Rigler, R.; Mets, U.; Widengren, J.; Kask, P. Fluorescence Correlation Spectroscopy with High Count Rate and Low Background: Analysis of Translational Diffusion. *Eur. Biophys. J.* **1993**, *22*, 169–175.
- (2) Kim, S. A.; Heinze, K. G.; Schwille, P. Fluorescence Correlation Spectroscopy in Living Cells. *Nat. Methods* **2007**, *4*, 963–973.
- (3) Levene, M. J.; Korlach, J.; Turner, S. W.; Foquet, M.; Craighead, H. G.; Webb, W. W. Zero-Mode Waveguides for Single-Molecule Analysis at High Concentrations. *Science* **2003**, *299*, 682–686.
- (4) Ruckstuhl, T.; Seeger, S. Attoliter Detection Volumes by Confocal Total-Internal-Reflection Fluorescence Microscopy. *Opt. Lett.* **2004**, *29*, 569–571.
- (5) Kastrup, L.; Blom, H.; Eggeling, C.; Hell, S. W. Fluorescence Fluctuation Spectroscopy in Subdiffraction Focal Volume. *Phys. Rev. Lett.* **2005**, *94*, 178104.
- (6) Rigneault, H.; Capoulade, J.; Dintinger, J.; Wenger, J.; Bonod, N.; Popov, E.; Ebbesen, T. W.; Lenne, P.-F. Enhancement of Single-Molecule Fluorescence Detection in Subwavelength Apertures. *Phys. Rev. Lett.* **2005**, *94*, 117401.
- (7) Borejdo, J.; Calander, N.; Gryczynski, Z.; Gryczynski, I. Fluorescence Correlation Spectroscopy in Surface Plasmon Coupled Emission Microscope. *Opt. Express* **2006**, *14*, 7878–7888.
- (8) Vobornik, D.; Banks, D. S.; Lu, Z.; Fradin, C.; Taylor, R.; Johnston, L. J. Fluorescence Correlation Spectroscopy With Sub-Diffraction-Limited Resolution Using Near-Field Optical Probes. *Appl. Phys. Lett.* **2008**, *93*, 163904.
- (9) Enderlein, J. A New Approach to Fluorescence Spectroscopy of Individual Molecules on Surfaces. *Phys. Rev. Lett.* **1999**, *83*, 3804–3807.
- (10) Roy, R.; Hohng, S.; Ha, T. A Practical Guide to Single Molecule FRET. *Nat. Methods* **2008**, *5*, 507–516.
- (11) Förster, T. Transfer Mechanisms of Electronic Excitation. *SPIERS Memorial Lecture* **1959**, *10*, 7–17.
- (12) Krichevsky, O.; Bonnet, G. Fluorescence Correlation Spectroscopy: the Technique and Its Applications. *Rep. Prog. Phys.* **2002**, *65*, 251–297.
- (13) Wenger, J.; Rigneault, H. Photonic Methods to Enhance Fluorescence Correlation Spectroscopy and Single Molecule Fluorescence Detection. *Int. J. Mol. Sci.* **2010**, *11*, 206–221.
- (14) Limozin, L.; Sengupta, K. Quantitative Reflection Interference Contrast Microscopy (RICM) in Soft Matter and Cell Adhesion. *ChemPhysChem* **2009**, *10*, 2752–2768.
- (15) Hu, K.; Ji, L.; Applegate, K. T.; Danuser, G.; Waterman-Storer, C. M. Differential Transmission of Actin Motion Within Focal Adhesions. *Science* **2007**, *315*, 111–115.
- (16) Wang, X.; et al. Non-Blinking Semiconductor Nanocrystals. *Nature* **2009**, *459*, 686–689.

Nonradiative Excitation Fluorescence: Probing Volumes Down to the Attolitre Range

Pascale Winckler, Rodolphe Jaffiol, Jérôme Plain* and Pascal Royer*

Laboratoire de Nanotechnologie et d'Instrumentation Optique, LRC CEA, CNRS UMR 6279 - STMR,
Institut Charles Delaunay, Université de Technologie de Troyes, 12 rue Marie Curie, BP 2060, 10 010
Troyes cedex, France

*Corresponding authors: rodolphe.jaffiol@utt.fr or jerome.plain@utt.fr

1 Material and methods

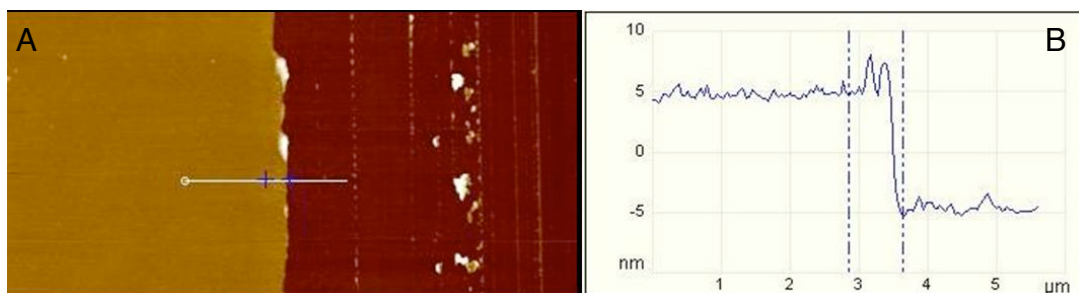
1.1 Preparation of the activated surface for FRET illumination

The Quantum dots (QDs) are core-shell CdSe/ZnS (Evident Technologies, FortOrange) with an emission peak at 600nm and a quantum yield which tends to be 100% in PMMA.¹² The total diameter of the QDs is $\approx 8\text{nm}$, with a core diameter about 4nm. A concentrated solution of quantum dots diluted in toluene ($\approx 0.5\mu\text{M}$) is added to a PMMA solution in toluene (2.5 g/L). QD-doped PMMA thin film is then obtained by spin-coating on cover glass

¹ Brokmann,X.; Coolen, L.; Hermier, J-P. and Dahan, M. Emission Properties of Single CdSe/ZnS Quantum Dots Close to a Dielectric Interface. *Chem. Phys.* **2005**, 318, 91-98.

² Brokmann, X.; Coolen, L.; Dahan M. and Hermier, J-P. Measurement of the Radiative and Non Radiative Decay Rates of Single CdSe Nanocrystals Through a Controlled Modification of their Spontaneous Emission. *Phys. Rev. Lett.* **2004**, 93, 107403.

at 3000 rpm. As shown Fig. S1, the thickness of the resulting film is 9 ± 1 nm (measured by AFM, Atomic Force Microscopy), indicating that a quasi-monolayer of quantum dots has been deposited on the substrate.^{3,4}



S 1 : (A) typical atomic force microscopy picture of the activated glass surface. On the left, a step created in the film. (B) The topography profile along the white line in the picture (A).

1.2 Fluorescent molecules

For fluorescence correlation spectroscopy (FCS) studies we used Alexa647 fluorescent molecules (Alexa647 carboxylic acid/succinimidyl ester, Invitrogen, A20006). In water, the optimal absorption of Alexa647 is 649nm, and its peak emission is situated at 664nm. For the observations of cell adhesion, we used a conventional plasma membrane fluorescent probe for red wavelength investigations, DiD (DiI_{C18}(5) oil, Invitrogen, D307). Absorption and emission peaks of DiD bound to phospholipid bilayer membrane are measured at 648nm and 670nm, respectively.

1.3 Cell culture and preparation

For adhesion studies, we used MCF-7 human breast cancer cells. They were grown in steril activated glass-based Petri dishes in RPMI-1640 medium (Gibco) enriched with 10% of fetal calf serum (Gibco) at 37°C and in a CO₂ humidified atmosphere of 5%. After, cells are labeled with a solution of DiD (20 μL of DiD diluted in ethanol (50 μM) added in 2 mL of aqueous solution which contain cells) during several hours in the CO₂ incubator. Finally,

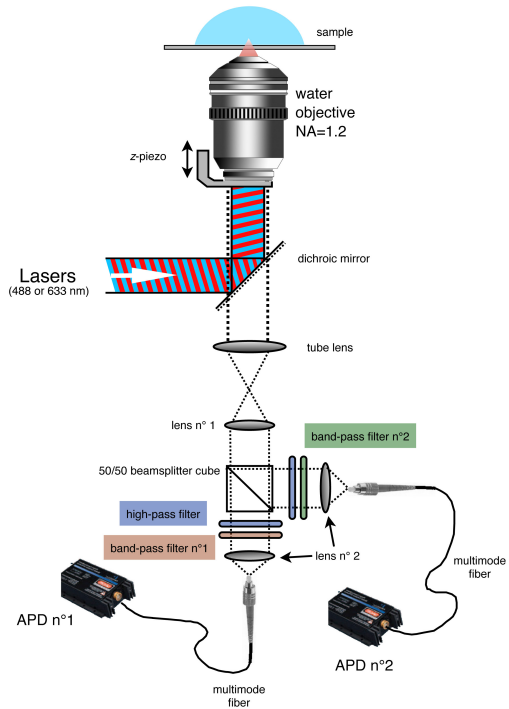
³ Plain, J.; Sonnefraud, Y.; Viste, P.; Lérondel, G.; Huant, S. and Royer, P. Self-assembly Drives Quantum Dot Photoluminescence, *J. of Fluorescence* **2009**, *19*, 311-316.

⁴ Viste, P.; Plain, J.; Jaffiol, R.; Vial, A.; Adam, P-M. and Royer P. Enhancement and Quenching Regimes in Metal-Semiconductor Hybrid Optical Nanosources. *ACS nano* **2010**, *4*, 759-764.

fluorescence observations were performed at room temperature in PBS (Gibco) in order to avoid the background signal related to the growth medium.

1.4 FCS setup

Our optical device for FCS measurements is based on a standard backscattering confocal microscope (a modified IX70 Olympus microscope), as schematically presented in Fig. S2. The excitation light is provided by two different laser lines, one at $\lambda=488$ nm (Sapphire 488 LP, Coherent), the other one at $\lambda=632.8$ nm (He-Ne laser, Thorlabs). After passing through a beam expander, the laser is reflected by a multiedge dichroic mirror (Semrock FF500/646-Di01) and strongly focused through a water immersion objective (Olympus UPlanSApo 60x, NA=1.2). Then, the fluorescence signal is collected through the same objective and after it is divided in two different detection channels with a 50/50 beamsplitter. Thus, by implementation of suited highly selecting filters, each channel can be dedicated to monitor the fluorescence of one molecule. In practice, one channel is devoted to



S 2 : Experimental setup for single molecule spectroscopy. Adapted with permission from Journal of Fluorescence, Springer.

the fluorescence of donor, i.e. the quantum dots (QDs), by combining a sharp high-pass filter (Semrock, LP02-488RU) and a selective band-pass filter centred on the QDs emission (Semrock FF01-600-14). The other

channel is dedicated to the fluorescence of acceptor, i.e. Alexa647, by an another set of filters (Semrock LP02-633RU and Semrock FF01-684-40). Finally, according to the total magnification of our microscope ($M=120$, $x60$ for the objective and $x2$ for the additional optical imaging system comprises lenses 1 and 2, see Fig. S2), two multimode fibers with a core diameter of $62.5\text{ }\mu\text{m}$ were used as point detector for confocal detection. The fluorescence signal is recorded with two similar avalanche photodiodes (PerkinElmer APD, SPCM-AQR-15) and then FCS was performed by a home made module.⁵

1.5 Wide-field Fluorescence imaging setup

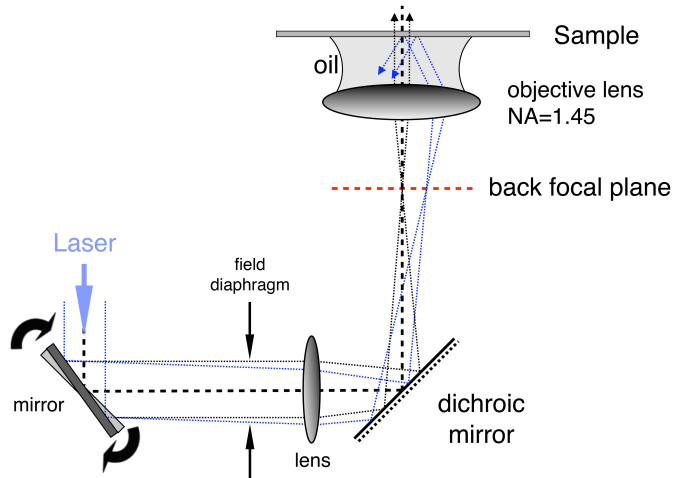
Our optical device for wide field imaging is a home made conventional prismless total internal reflection fluorescence microscope (TIRFM).⁶ The setup is based on an inverted microscope (IX71, Olympus). The laser excitation is provided by the 457 and 488nm lines of an Argon laser (Spectra-Physics 163C). The laser beam, previously collimated, is then focused with an appropriate lens onto the back focal plane of an oil-immersion objective (Olympus PlanApoN 60x, NA=1.45), as shown Fig. S3. A pivotable mirror mount is used to adjust the lateral position of the focusing on the periphery of the pupil entrance of the objective, thus allowing to generate internal reflection at the glass-water interface. The total internal reflection illumination is achieved when the angle between the parallel rays emerging from the objective and the glass-sample surface is greater than the critical angle, Fig. S3.⁷ By this way, the lateral dimension of the evanescent wave is adjusted with a field diaphragm located just before the focusing lens. The typical lateral illumination size is $\approx 100\times 100\text{ }\mu\text{m}^2$. The fluorescence light is collected by the same objective, and after passing a set of three filters (for the 457nm line : dichroics Semrock Di01-R442, high-pass filter Semrock LP02-473RS and for FRET imaging the additional band-pass filter Semrock FF01-684-40 ; for the 488nm line : dichroics Semrock Di01-R488, high-pass filter Semrock BLP-488R and for FRET imaging the additional band-pass filter Semrock FF01-684-40) the signal is directed to a high sensitive CCD camera (Photometrics, CoolSNAP HQ2). Such total internal reflection scheme gives the

⁵ Boutin, C.; Jaffiol, R.; Plain J. and Royer, P. Surface Modified Single Molecules Free-Diffusion Evidenced by Fluorescence Correlation Spectroscopy. *J. of Fluorescence* **2008**, *18*, 1115-1122.

⁶ Axelrod, D. Total Internal Reflection Fluorescence Microscopy (Chapter 9), *Methods in Cell Biology* **1989**, *30*, 245-270.

⁷ Hassler, K.; Leutenegger, M.; Rigler, P.; Rao, R.; Rigler, R.; Gösch M. and Lasser, L. Total Internal Reflection Fluorescence Correlation Spectroscopy (TIR-FCS) with Low Background and High Count-Rate per Molecule. *Optics Express* **2005**, *13*, 7415-7423.

opportunity to add simultaneously to this dark field evanescent illumination a bright field illumination to observe for example the contours of the cells, as on the movie of MCF-7 cell.



S 3 : Prismless total internal reflection illumination through the periphery of a high numerical aperture objective.

2 Results

2.1 Förster distance (R_0) calculation

The rate of nonradiative energy transfer k_{FRET} is given by the Förster formulation:⁸

$$k_{FRET} = \frac{1}{\tau_D} \left(\frac{R_0}{R} \right)^6 \quad (1)$$

$$\text{and } R_0 \sim 8.7853 \times 10^{-25} \frac{\kappa^2 \phi_D I_R}{n^4}$$

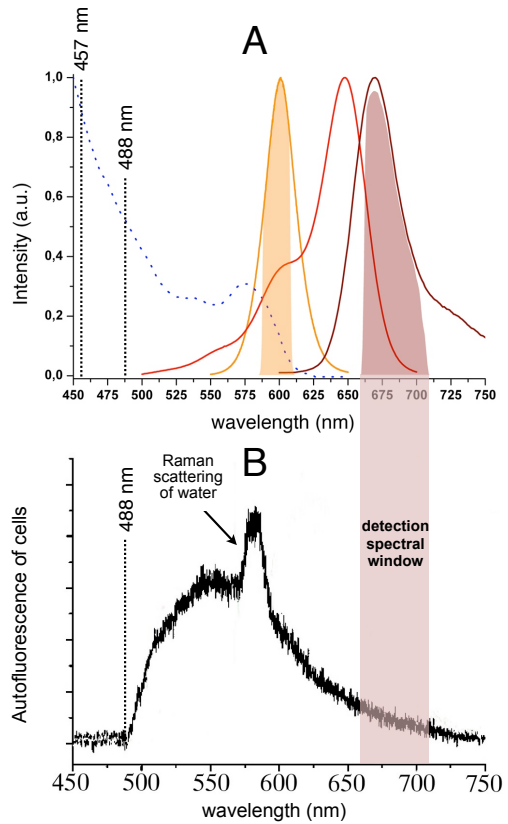
$$\text{with } I_R = \frac{\int d\lambda F_d(\lambda) \epsilon_a(\lambda) \lambda^4}{\int d\lambda F_d(\lambda)}$$

⁸ Cheung, H. C. Resonance Energy Transfer (Chap. 3) in Topic in Fluorescence Spectroscopy Volume 2 (ed. J. R. Lakowicz), Plenum Press, New York 1991.

In these formulae, τ_D is the donor lifetime in the absence of the acceptor, R is the donor-acceptor distance and R_0 the so called Förster distance. κ^2 is the orientation factor for dipole-dipole interaction. If the donor and acceptor can freely rotate, the orientation factor can be approximate by its averages value, $\langle \kappa^2 \rangle = 2/3$. Φ_D is the quantum yield of the donor in the absence of the acceptor, n is the refractive index of the medium. Finally, I_R is the normalized spectral overlap integral between donor emission (F_d) and molar extinction of acceptor (ε_a). $F_d(\lambda)$ is in arbitrary units, R , R_0 and λ in cm, the molar extinction $\varepsilon_a(\lambda)$ in the usual chemical unit, $M^{-1}cm^{-1}$. Since the quantum yield of the QDs FortOrange in PMMA tends towards 100%, we obtain for Alexa647 dyes in water as acceptor, a Förster distance $R_0 = 9.36$ nm.

2.2 Quantum dots spectral advantages for FRET applications in biology

In biological FRET applications the background signal has several origins. For an important part, it can be attributed to the autofluorescence of cells and also to the direct excitation of acceptors with the laser source. Less significantly, another source of background is due to Raman scattering of water and biological materials. The huge Stokes shift between the blue excitation of FortOrange-quantum dots and their orange-red emission spectrum allows to strongly diminish all these background signals. Indeed, by using a blue laser excitation at 457 or 488nm, we definitively avoid the direct excitation of acceptors during the FRET illumination process, as shown in Fig. S4A. Furthermore, if we reduce with a well-suited band pass filter the detection to a narrow spectral window centered on acceptor emission, it becomes possible to drastically eliminate the autofluorescence and Raman scattering generated within living cells, Fig. S4B. In addition, the nonradiative energy transfer increases the Stokes shift towards wavelength greater than 650nm, as indicated in Fig. S4. For example, with the 457nm laser line, the Stokes shift between the laser excitation and the peak emission of DiD molecules (the acceptors) is about 210nm.



S 4 : (A) Normalized absorption spectra of QDs (in blue dots) and of DiD (in red) ; normalized emission spectra of QDs (in orange) and of DiD (in dark red). The two colored parts indicate the two different detection spectral windows, in orange for the channel dedicated to QDs detection and dark red for the other channel dedicated to the DiD fluorescence emission. (B) Typical autofluorescence spectrum of MCF-7 cells recorded with an excitation wavelength at 488nm.

2.3 Size determination of the observation volume by FCS

Fluorescence Correlation Spectroscopy (FCS) is an experimental technique using statistical analysis of the fluctuation of fluorescence signal in order to decipher molecular events, such as diffusion or interactions of biomolecules. FCS is based on the temporal autocorrelation $G(\tau)$ of the collected fluorescence signal emitted by dyes diffusing or flowing through the observation volume V of the microscope. From the μsec to the sec time scale, the shape of the autocorrelation function $G(\tau)$ of single molecules freely diffusing for example in water depends essentially on the diffusion process and on the triplet state dynamics (and all other non-fluorescent

states).⁹ In this time range the amplitude of $G(\tau)$ is inversely proportional to the average number N of molecules simultaneously present in the observation volume, and the $G(\tau)$ decay time is relies on two characteristics times: the diffusion time τ_d and the triplet time τ_b . τ_d corresponds to the average time required for one molecule to cross the observation volume and τ_b is related to the different intramolecular radiative and nonradiative transition rate.¹⁰ An example of autocorrelation curve recorded with our confocal setup (Fig. S2) for a nanomolar solution of Alexa647 molecules freely diffusing in water, is presented in Fig. S5A. The experimental value of the diffusion time of Alexa647 is $39 \pm 0.5 \mu\text{s}$. In our study, experimental autocorrelation function was fitted with the following model describing free diffusion in an open volume, according to molecules diffusing in 2-D (that is observed with FRET illumination whenever molecule diffusing at the close vicinity of a surface) or in 3-D (for molecule diffusing far from the surface):⁵

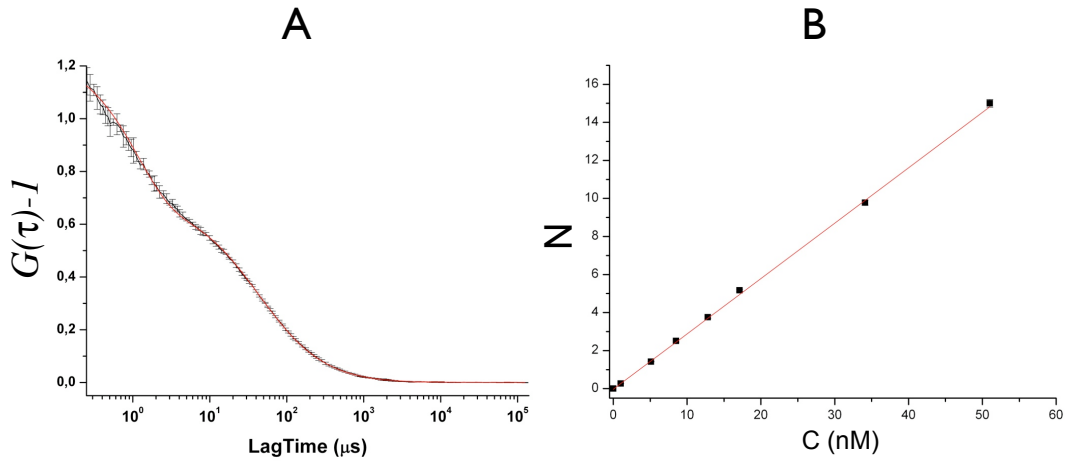
$$G_{2D}(\tau) = 1 + \frac{1}{N} \left(1 - \frac{B}{F}\right)^2 \frac{1 + \frac{b}{1-b} e^{-\frac{\tau}{\tau_b}}}{1 + \frac{\tau}{\tau_d}} \quad (2)$$

$$G_{3D}(\tau) = 1 + \frac{1}{N} \left(1 - \frac{B}{F}\right)^2 \frac{1 + \frac{b}{1-b} e^{-\frac{\tau}{\tau_b}}}{\left(1 + \frac{\tau}{\tau_d}\right) \left(1 + \frac{\tau}{S^2 \tau_d}\right)^{\frac{1}{2}}} \quad (3)$$

where b is the fraction of molecule in a non fluorescent state (i.e. the triplet state). B and F are respectively the background noise and the total intensity detected with APD. To quantify the accurate size of the confocal observation volume, we plot the mean number of molecule obtained by fitting the autocorrelation functions according to eq. (3), as a function of the concentration of the dye solution. We obtained for our confocal setup and Alexa647 solutions the plot presented in Fig. S5(B). Since $N=C \cdot V$, it is easy to extract from the slope of the plot, the accurate size of the observation volume V . Thus we have obtained $V=0.428 \pm 0.003 \mu\text{m}^3$ at 632.8nm.

⁹ Krichevsky, O. and Bonnet, G. Fluorescence Correlation Spectroscopy: the Technique and its Applications, *Rep. Prog. Phys.* **2002**, *65*, 251-297.

¹⁰ Widengren, J.; Mets, U. and Rigler, R. Fluorescence Correlation Spectroscopy of Triplet States in Solution: a Theoretical and Experimental Study, *J. Phys. Chem.* **1995**, *99*, 13368-13379.



S 5 : (A) Typical autocorrelation curve recorded on a nanomolar solution of Alexa647 in water ($C=5.8\text{nM}$). The laser power at 632.8nm , measured at the pupil entrance of the objective is $30 \mu\text{W}$ (the experimental setup is describe in section 1.4). This autocorrelation function results from the average of five autocorrelation curves recorded consecutively, each during 30sec . Red curve: fit according to eq. 3. (B) Plot of the mean number of molecule N versus the concentration C . Red curve: the linear fit.

2.4 Signal to noise ratio in FRET illumination

Observing single molecules within a high concentrated solution of dye need to carefully optimize the signal-to-noise ratio. In single molecule detection, the signal-to-noise can be written as follows:^{11,12}

$$SNR = \frac{\sqrt{S}}{\sqrt{1 + \frac{B}{S}}} \quad (4)$$

$$S = \eta_C k_{FRET} \phi_A \quad (5)$$

$$B = B_d + \eta_C V(n_{matrix} \sigma_{Raman} + n_{protein} \sigma_{Autofluo} + C_A N \sigma_{abs} \phi_A) \left[\frac{I}{h\nu} \right]_{laser} \quad (6)$$

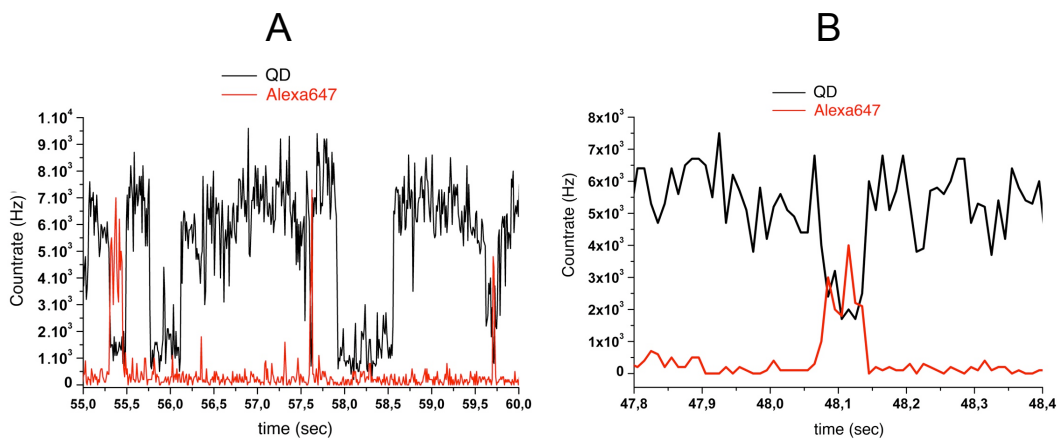
S is the signal of acceptor through a FRET excitation and B is the total background signal, both expressed in counts per second (i.e. count rate in Hz). A small background-to-signal ratio (B/S) results in an optimal SNR which depends only on the square root of the count rate S (i.e. a shot-noise limited signal). η_C is the collection

¹¹ Azoulay, J.; Débarre, A.; Jaffiol, R. and Tchénio, P. Original Tools for Single-Molecule Spectroscopy. *Single Mol.* **2001**, 2, 241-249.

¹² Michalet, X. and Weiss, S. Single-Molecule Spectroscopy and Microscopy. *C.R. Physique* **2002**, 3, 619-644.

efficiency, Φ_A the fluorescence quantum yield of acceptor, V the probe volume, I the laser intensity (in W/cm²) and $h\nu$ the laser excitation energy. B_d is the detector dark count rate (typically 50Hz for APD). σ_{Raman} , $\sigma_{Autofluo}$ and σ_{abs} are respectively the Raman cross-section of the biological matrix, the autofluorescence cross-section of proteins or any other fluorescent biomolecules present in living cells and the absorption cross-section of acceptor. n_{matrix} and $n_{protein}$ are respectively the number per unit-volume of biomolecules which give rise to Raman scattering and autofluorescence. C_A is the concentration of acceptor and N the Avogadro constant.

First of all, a strong reduction of the probe volume V can decrease broadly the background signal, and so increase the signal-to-noise ratio, equations (4) and (5). Moreover, by using an appropriate spectral filtering, it is possible to eliminate to a large extent the Raman scattering and the autofluorescence of cells, as shown Fig. S4. Finally, the main residual source of background signal in our experiment is related to the direct excitation of acceptors with the laser beam (the last term in the parenthesis of eq(6)). As previously explained in section 2.1, this last background signal can be removed if the laser excitation wavelength is significantly far from the absorption band of acceptor, that can be achieved with QDs as donors, Fig. S4. In the case of FCS experiments with high concentrated solution of Alexa647 molecules, as in the experiment presented in the Fig. 2A in the main text, the background signal related to the direct excitation of Alexa647 at 488nm is ≈ 170 Hz. Adding the dark count of the APD, we obtain a total background of about 220 Hz, which corresponds approximatively to 10 % of the total count rate detected. This last point highlights the key aspect of quantum dots as donors in our FRET illumination scheme. Another experiment can illustrate the excellent SNR of our optical setup, see Fig. S6. In this case, we observe the FRET between a single QD excited at 488nm, and Alexa647 molecules freely diffusing around it. Fig. S5 (A) and (B) show anticorrelated two-state fluctuations between signals through the donor and acceptor channels.



S 6 : Two examples of fluorescence time trace recorded with our confocal setup at 488nm with a laser of 110nW measured at the pupil entrance of the objective (see section 1.4), on a single quantum dot recovered by a droplet of a solution of Alexa647 in water (C=50nM). In black the photoluminescence of the single QD recorded through the donor detection channel and in red the fluorescence signal of Alexa647 molecules, recorded simultaneously through the acceptor detection channel.

Another limitation to the signal-to-noise ratio in FRET illumination is related to the photoluminescence intermittency of single quantum dots, well known as «blinking», Fig. S6. As shown by Chevalier et al., the blinking could be overpassed if more than three QDs are present in the detection volume.¹³ In our FCS experimental conditions we excite simultaneously typically tens QDs with the focused laser beam (see sections 1.1 and 1.4). In this case, the FRET illumination is statically continuously and homogeneously operating within the laser focal spot. Furthermore, non-blinking QD recently reported in the literature will be used as donor in forthcoming experiments.¹⁴

¹³ Chevalier, N.; Nasse, M.J.; Woehl, J.C.; Reiss, P.; Bleuse, J.; Chandeson, F. and Huant S. CdSe Single-Nanoparticle Based Active Tips for Near-Field Optical Microscopy. *Nanotechnology* **2005**, *16*, 613-618.

¹⁴ Wang X. et al. Non-Blinking Semiconductor Nanocrystals, *Nature* **2009**, *459*, 686-689.